SUPPLEMENTARY MATERIAL

Design and synthesis of AIE-active naphthaldehyde hydrazone-based ligand: Mechanochromic, acidochromic, and sensing studies

Ram Kumar Mandal[a], Pankaj Haloi[a], Abhinav Jain[a], Sourav Sutradhar[a], Jebiti Haribabu[b], Diego Quezada[c], Daniel Moraga[d], Pranjit Barman[a] *

[a] Department of Chemistry, National Institute of Technology Silchar, Silchar, Cachar-788010 Assam

[b] Faculty of medicine, University of Atacama, Los Carreras 1579, 1532502, Copiapo, Chile

[c]Facultad de Ingenieria, Instituto de Ciencias Aplicadas, Universidad Autonoma de Chile, Del Valle 534, Huechuraba, Santiago, Chile

[d]Laboratorio de Fisiología, Departamento de Ciencias Biomédicas, Facultad de Medicina, Universidad de Tarapacá, Arica 1000000, Chile

Chemicals

2-Hydroxy-1-naphthaldehyde and 3,5-difluoro-salicylaldehyde were purchased from Alfa Aesar, and hydrazine hydrate (80%) was purchased from Thermo Fisher Scientific. A range of organic solvents (methanol, ethanol, THF, DCM, DMF, DMSO, $CHCl_3$, acetonitrile and, hexane, along with metal salts such as $Cu(NO_3)_2 \cdot 3H_2O$, $Al(NO_3)_3$, $Zn(NO_3)_2$, $Cd(NO_3)_2$, $Pb(NO_3)_2$, NaCl, KCl, $MgCl_2$, $CaCl_2$, $CoCl_2 \cdot 6H_2O$, $SnCl_2$, $NiCl_2$, and $FeCl_3$ were sourced from Merck and BLD Pharm. All reagents were used exactly as supplied without any further additional purification.

Instrumentation

FT-IR spectra were recorded on a Bruker ALPHA Spectrometer as KBr diluted disks. ^1H NMR spectra were obtained using a JEOL JNM ECS400 spectrometer operating at 400 MHz in $CDCl_3$, with chemical shifts (δ) reported in ppm relative to TMS as an internal standard. ESI-MS measurements were carried out on an XEVOG2 XS QTOF spectrometer. Ultraviolet–visible absorption spectra were recorded using a Genesys 10S spectrophotometer, while

photoluminescence emission spectra were recorded on a HITACHI F-4600 spectrophotometer. Powder X-ray diffraction (PXRD) diffractograms were utilized using Rigaku Ultima-IV powder X-ray Diffractometer (with SAXS attachment).

Computational studies:

Computational studies were performed using GAUSSIAN 16 software. The ground-state geometries of the ligand and complex structures were optimized by density functional theory (DFT) [1,2]employing the LanL2DZ basis set for the metal centre and the 6-31+G(d,p) basis set for the remaining atoms, with the B3LYP functional[3,4].

Calculation of limit of detection (LOD)

The limit of detection (LOD) for **L2** in the presence of Cu^{2+} ions was determined using fluorescence titration data. It was calculated using the equation-

$$LOD=3\sigma/S \quad (1)$$

where σ represents the standard deviation of the blank measurements, and S is the slope of the calibration plot of ($I_0 - I$) versus Cu^{2+} concentration. Here, I_0 and I correspond to the emission intensities of the ligand in the absence and presence of copper ions, respectively [5].

Calculation of binding constant (Kb)

The binding constant was calculated from the fluorometric titration data using the Benesi–Hildebrand approach. It was evaluated by applying the following equation-

$$1/I\ Io=[1Imax\ Io]/[1Kb\cdot C+1] \quad (2)$$

In this equation, I_0 represents the emission intensity of free **L2**, while I corresponds to the fluorescence intensity of **L2** recorded at different equivalents of Cu^{2+}. The value I_{max} refers to the maximum emission intensity obtained after adding 2 equivalents of Cu^{2+} to the sensor. The term C indicates the concentration of the Cu^{2+} ions used [6].

Calculation of Stern-Volmer constant (Ksv)

The extent of fluorescence quenching caused by the addition of Cu^{2+} ions was evaluated using the Stern–Volmer equation [7]. It is expressed as follows-

$$Io\ /I=1+K_{SV}\times[Cu^{2+}] \quad (3)$$

Where Ksv is the Stern-Volmer constant and Io and I stand for emission intensities at various concentrations with and without Cu^{2+}ions.

Cell culture

HeLa cells were cultured in Dulbecco's Modified Eagle Medium (DMEM) containing 10% fetal bovine serum (FBS) and kept at 37 °C in a 5% CO_2 atmosphere. The cells were then seeded onto 18 mm glass coverslips and allowed to attach for 24 hours.

Cytotoxicity assay

The cytotoxicity of **L2** toward HeLa cells was assessed using the MTT assay. Different concentrations of **L2** and the L2–Cu^{2+} complex (0–100 μM) were added to the wells of a 96-well plate containing cultured cells. The plate was then incubated for 24 h at 37 °C in a 5% CO_2 environment. After incubation, 10 μL of MTT solution (5 mg/mL) was added to each well, followed by an additional 4-hour incubation under the same conditions. Absorbance was recorded at 440 nm using a Multiskan GO microplate reader. Cell viability was determined using the formula:

Cell viability (%) = (mean absorbance of treated wells) / (mean absorbance of control wells).

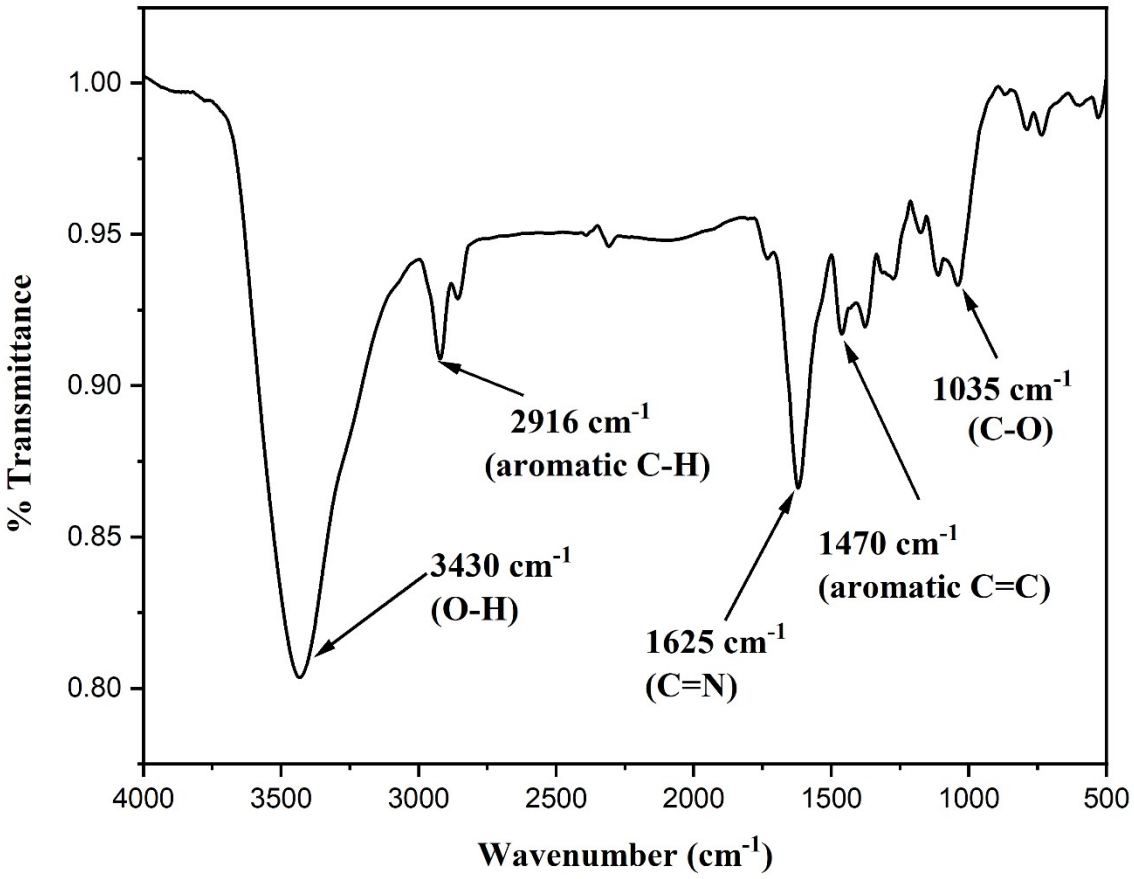

Fig. S1. FTIR spectra of Schiff base ligand **L2**

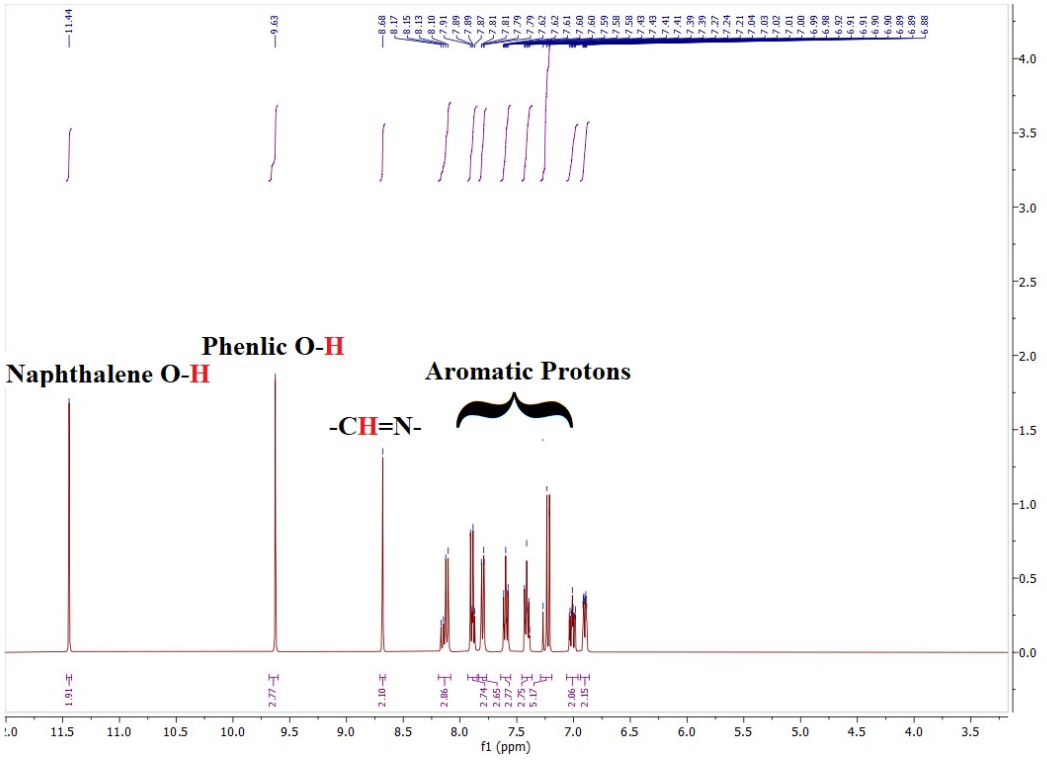

Fig.S2. ^{1}H NMR spectra of Schiff base ligand **L2**

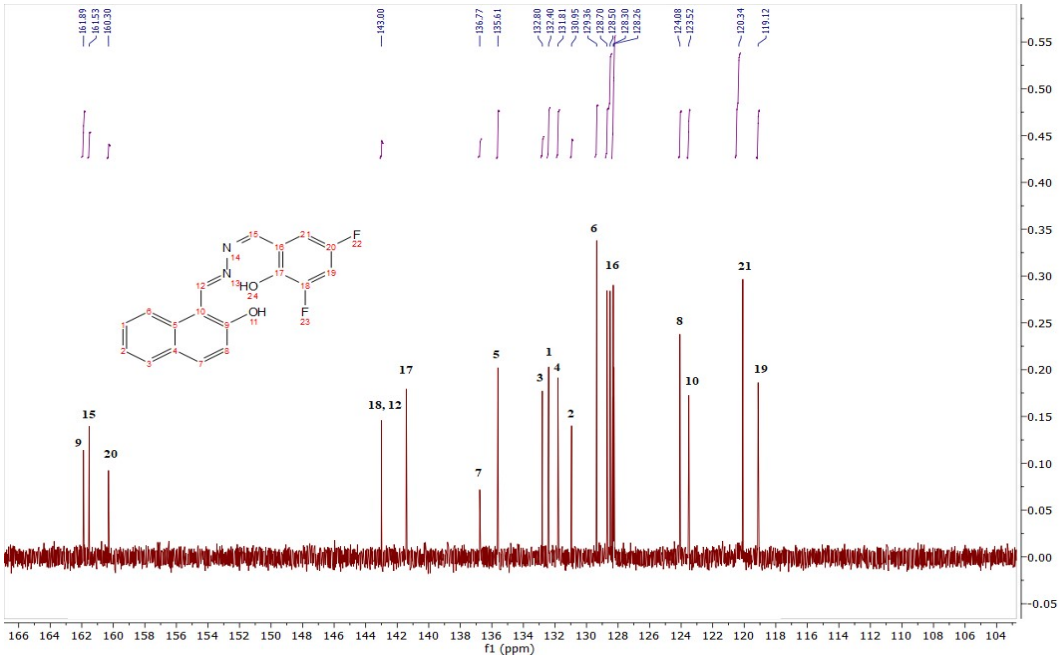

Fig.S3. ^{13}C NMR spectra of Schiff base ligand **L2**

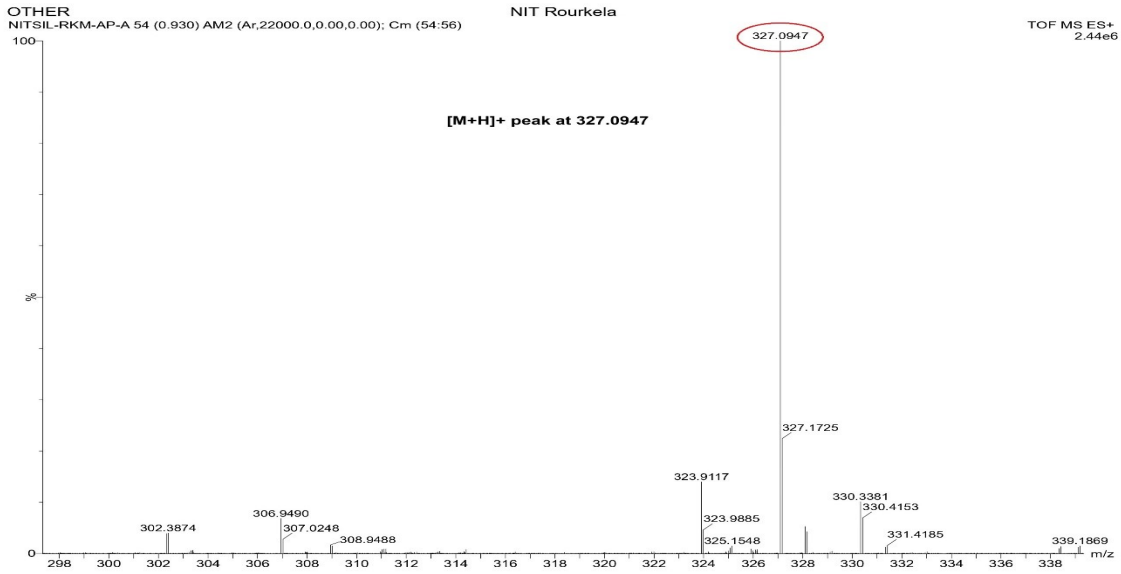

Fig.S4. ESI-MS spectra of Schiff base ligand **L2**

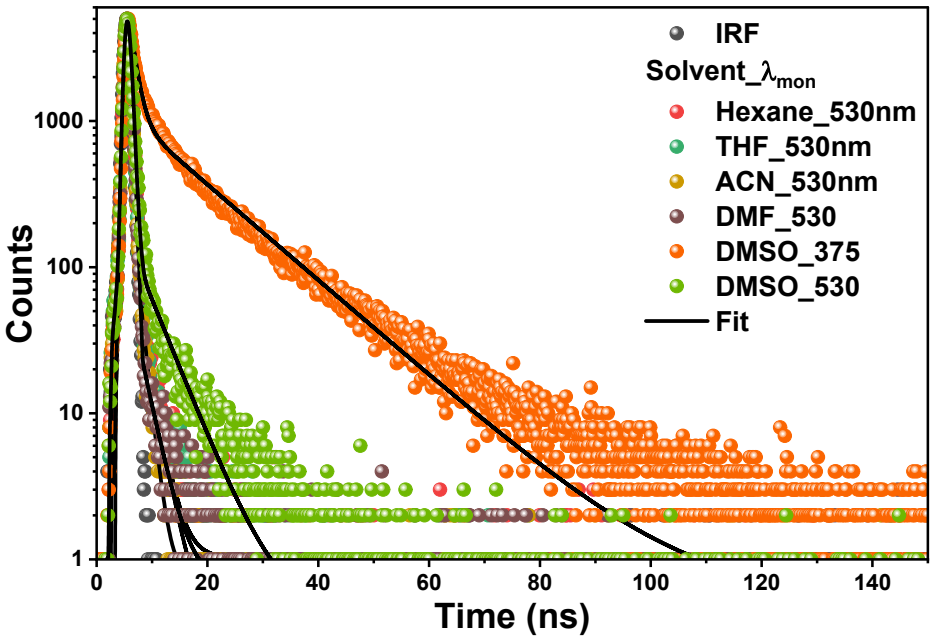

Fig. S5**.** Lifetime plots of **L2** in different solvents.

Table S1: Photophysical properties of **L2** (50μM) in different solvents.

Solvents	$\lambda_{abs\ (nm)}$[a]	$\lambda_{em\ (nm)}$[b]	**Stokes Shift (nm/cm^{-1})**[c]	τ_1 **(ns)**	A_1 **(%)**	τ_2 **(ns)**	A_2 **(%)**	τ_{avg} **(ns)**[d]	χ^2

DMF	334, 392	374, 526	192/10929	0.05	99.41	2.39	0.59	0.602	1.03
DMSO	335, 390	376, 534	200/11160	1.15, 0.23	37.29, 92.85	13.25, 4.6	62.71, 7.15	0.99 0.97	1.08 1.08
ACN	333, 399	374, 530	197/11160	0.013	99.99	1.2	0.01	0.026	1.07
THF	334, 399	375, 532	198/11137	0.09	97.76	1.97	2.24	0.71	1.06
n-HEX	329, 394	529	200/11500	0.08	98.10	1.95	1.90	0.679	1.02

[a] The absorption maximum in nm.

[b] The emission maximum of E-E* (left) and K-K* (right) in nm.

[c] Stokes shift calculated from absorption maximum to K-K* emission.

[d] **The average lifetime of E-E* (left) and K-K* (right), using standard ∑ notation**

$$\pi_{avg} = \frac{\sum_{i=1}^{n} A^{*}(\tau_i)^2}{\sum_{i=1}^{n} \left(A^{*}_{i} \tau_i\right)} \quad \textbf{..... (1)}$$

Where:

- A_i is relative abundance and
- τ_i is the lifetime of the i^{th} component.

Amplitude-weighted average lifetimes using standard Σ notation:

$$I_{f_{it}}(t) = \sum_{i=1}^{n} A_i \exp\left(-\frac{t}{\tau_i}\right) \quad \text{..... (2)}$$

where:

- A_i is the amplitude (or amplitude fraction) and
- τ_i are lifetime components.

Standard equation for χ^2:

$$X^2 = \frac{1}{N-P}\sum_{j=1}^{N}\left[\frac{I_{exp}(t_j) - I_{fit}(t_j)}{\sigma_j}\right]^2 \quad \text{..... (3)}$$

where:

- $I_{\text{exp}}(t_j)$= experimental fluorescence intensity at time t_j
- $I_{\text{fit}}(t_j)$= fitted intensity obtained from the decay model
- σ_j= standard deviation (error) of the experimental data at t_j
- N= total number of time channels (data points)
- p= number of fitted parameters (e.g., A_i, τ_i)

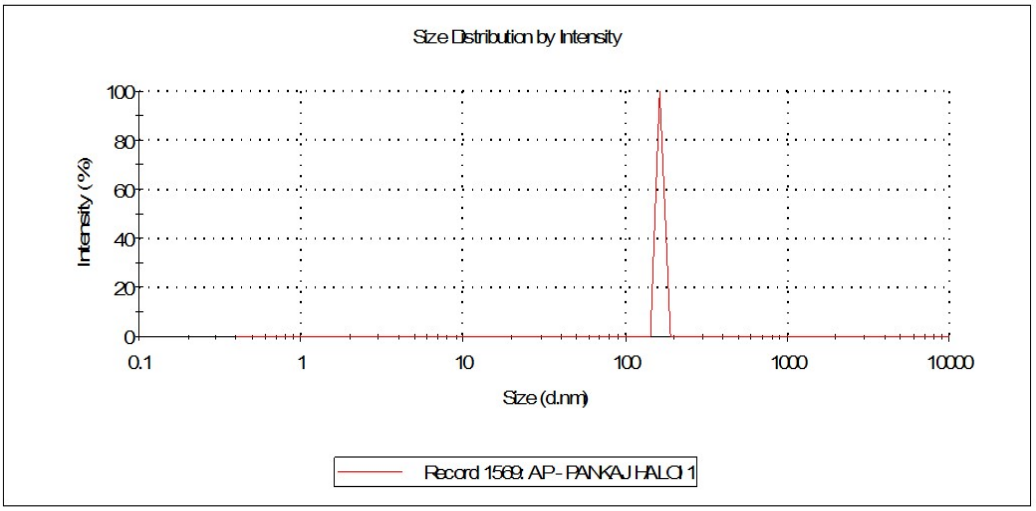

Fig.S6. DSL data of L2 sensor at 90% THF: water fraction

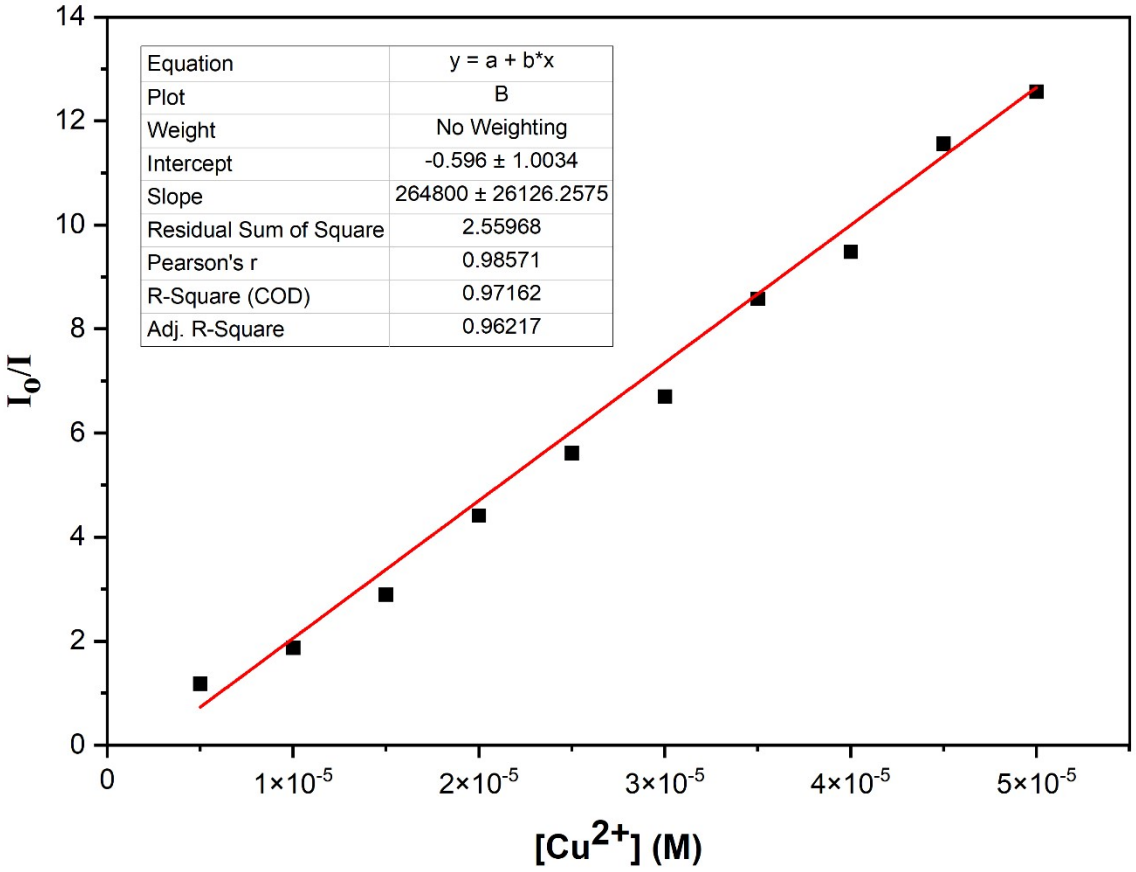

Fig.S7. Stern-Volmer plot for sensor **L2**

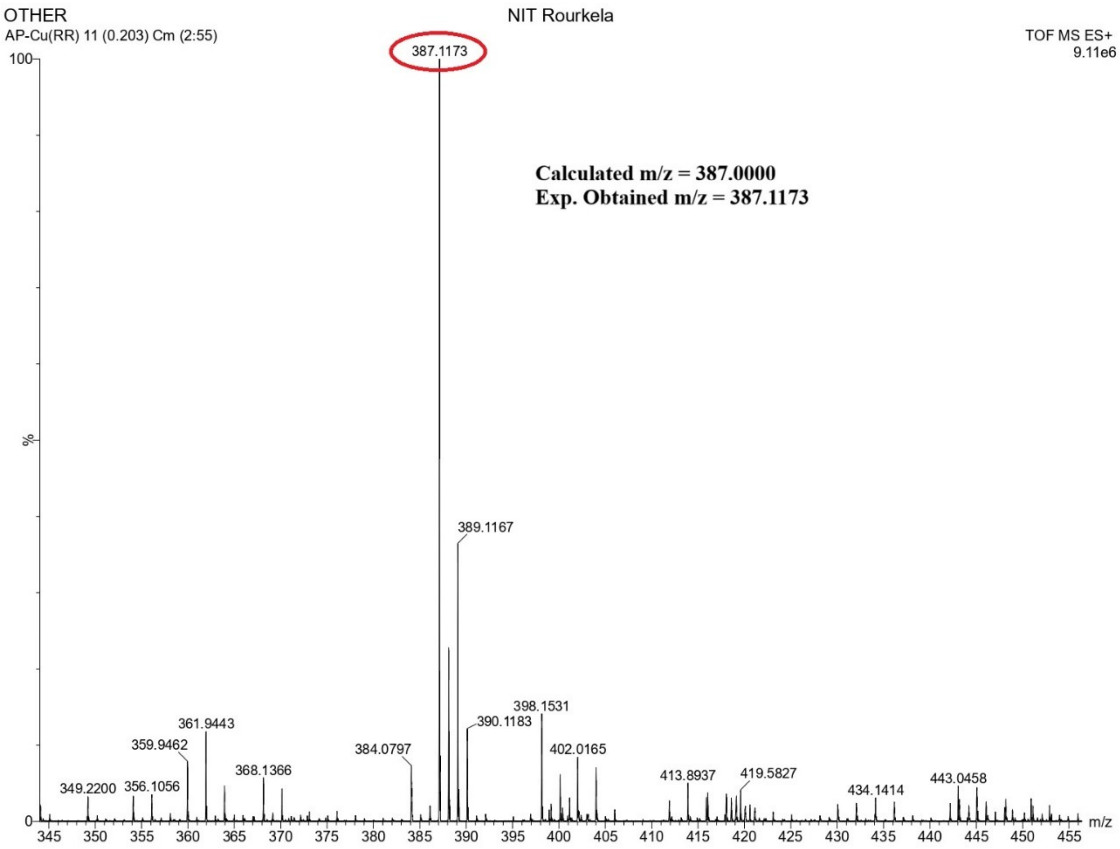

Fig.S8. ESI-MS spectra of Schiff base **L2**-Cu^{2+}

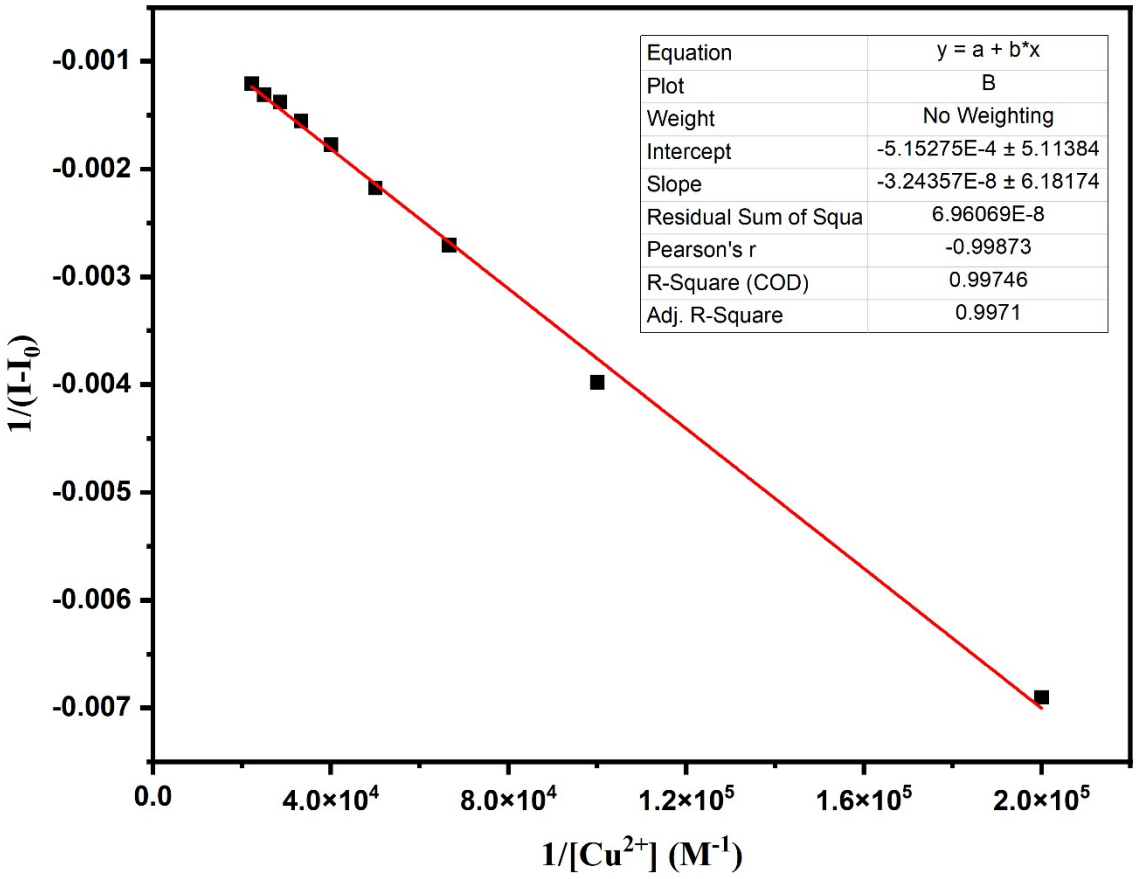

Fig.S9. Benesi-Hildebrand plot of 1/I-I0 versus $1/[Cu^{2+}]$

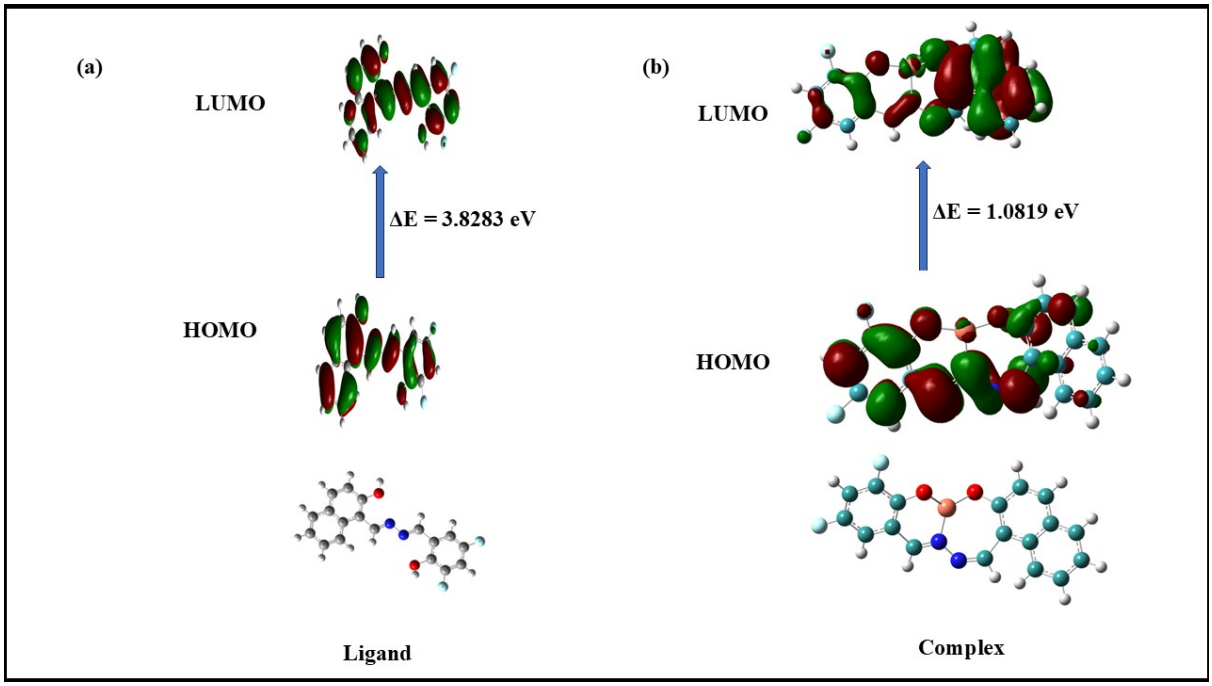

Fig.S10. Optimized structure and HOMO-LUMO energy diagram of **L2** and **L2**-Cu^{2+} complex

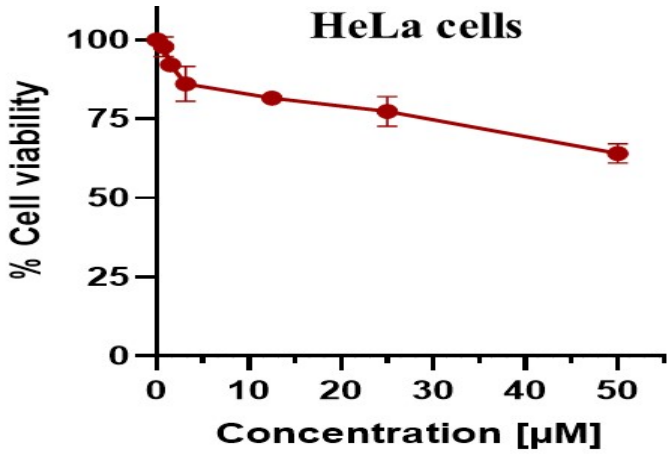

Fig.S11. Cytotoxicity assay for sensor L2 towards HeLa cells in different concentrations of Cu^{2+} ions.

Table S2 Bond lengths (Å) of **L2**

Number	Atom1	Atom2	Length
1	F1	C7	1.356(4)

2	F2	C12	1.363(4)
3	O1	H1	0.82
4	O1	C9	1.349(4)
5	O2	H2	0.82
6	O2	C10	1.349(4)
7	N1	N2	1.397(3)
8	N1	C5	1.277(4)
9	N2	C2	1.286(4)
10	C1	C5	1.448(3)
11	C1	C6	1.387(4)
12	C1	C9	1.404(4)
13	C2	H2A	0.93
14	C2	C4	1.447(3)
15	C3	C4	1.437(4)
16	C3	C11	1.420(3)
17	C3	C13	1.408(4)
18	C4	C10	1.380(4)
19	C5	H5	0.929
20	C6	H6	0.93
21	C6	C7	1.367(3)
22	C7	C8	1.362(4)
23	C8	H8	0.93
24	C8	C12	1.353(4)
25	C9	C12	1.383(3)
26	C10	C18	1.412(4)
27	C11	C14	1.409(5)
28	C11	C15	1.412(6)
29	C13	H13	0.93
30	C13	C17	1.363(5)
31	C14	H14	0.93
32	C14	C16	1.341(6)
33	C15	H15	0.93

34	C15	C18	1.338(5)
35	C16	H16	0.93
36	C16	C17	1.396(4)
37	C17	H17	0.93
38	C18	H18	0.93

Table S3 Bond angles (°) of **L2**

Number	**Atom1**	**Atom2**	**Atom3**	**Angle**
1	H1	O1	C9	109.5
2	H2	O2	C10	109.5
3	N2	N1	C5	114.2(2)
4	N1	N2	C2	112.2(2)
5	C5	C1	C6	119.6(2)
6	C5	C1	C9	121.0(2)
7	C6	C1	C9	119.4(2)
8	N2	C2	H2A	118.9
9	N2	C2	C4	122.2(2)
10	H2A	C2	C4	118.9
11	C4	C3	C11	118.9(2)
12	C4	C3	C13	124.1(2)
13	C11	C3	C13	117.0(2)
14	C2	C4	C3	119.9(2)
15	C2	C4	C10	120.6(2)
16	C3	C4	C10	119.4(2)
17	N1	C5	C1	120.5(2)
18	N1	C5	H5	119.8
19	C1	C5	H5	119.8
20	C1	C6	H6	120.2
21	C1	C6	C7	119.6(2)
22	H6	C6	C7	120.2

23	F1	C7	C6	119.2(2)
24	F1	C7	C8	118.3(2)
25	C6	C7	C8	122.5(3)
26	C7	C8	H8	121.3
27	C7	C8	C12	117.3(3)
28	H8	C8	C12	121.4
29	O1	C9	C1	124.3(2)
30	O1	C9	C12	118.5(2)
31	C1	C9	C12	117.2(2)
32	O2	C10	C4	123.4(3)
33	O2	C10	C18	115.8(3)
34	C4	C10	C18	120.8(3)
35	C3	C11	C14	119.5(3)
36	C3	C11	C15	118.4(3)
37	C14	C11	C15	122.1(3)
38	F2	C12	C8	118.8(3)
39	F2	C12	C9	117.2(2)
40	C8	C12	C9	124.0(3)
41	C3	C13	H13	119.2
42	C3	C13	C17	121.6(3)
43	H13	C13	C17	119.2
44	C11	C14	H14	119.2
45	C11	C14	C16	121.8(3)
46	H14	C14	C16	119.1
47	C11	C15	H15	118.7
48	C11	C15	C18	122.5(3)
49	H15	C15	C18	118.7
50	C14	C16	H16	120.3
51	C14	C16	C17	119.4(3)
52	H16	C16	C17	120.3
53	C13	C17	C16	120.8(3)
54	C13	C17	H17	119.6

55	C16	C17	H17	119.6
56	C10	C18	C15	119.9(3)
57	C10	C18	H18	120
58	C15	C18	H18	120.1

Table S4. A comparative analysis of previously reported naphthaldehyde hydrazone-based Schiff base ligand.

Ligand Structure	**AIE Behaviour**	**Mechanochromic, or Acidochromic properties**	**Metal Ion Sensing**	**LOD Value**	**Ref.**
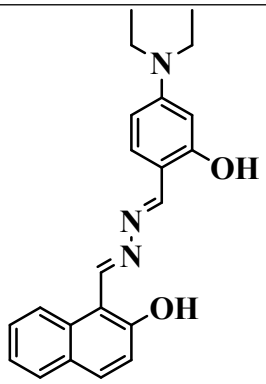	Yes	Mechanochromic	Cu^{2+}, Al^{3+}	$1.52x10^{-7}$ $1.65x10^{-7}$	8
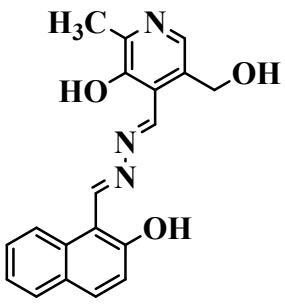	Yes	No	Cu^{2+}	$0.33x10^{-7}$	9
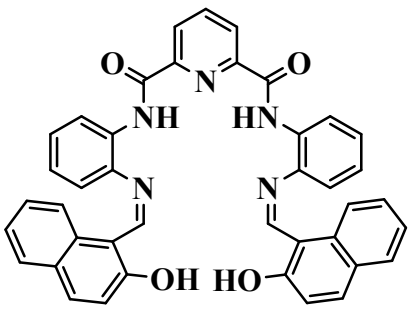	Yes	Mechanochromic	Cu^{2+}	$1.8x10^{-7}$	10

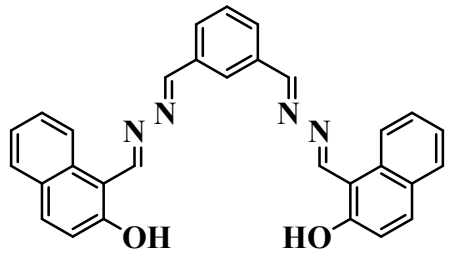	Yes	No	Cu^{2+}	$16x10^{-15}$	11
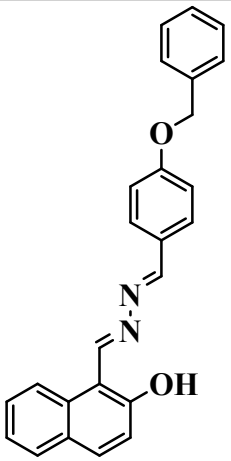	Yes	No	Cu^{2+}	$0.35x10^{-7}$	12
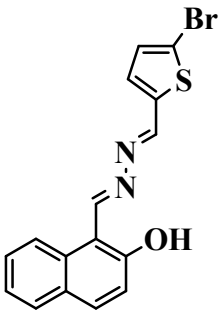	No	No	Cu^{2+}	$28x10^{-7}$	13
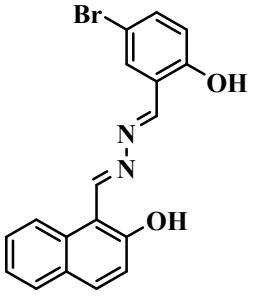	Yes	No	Al^{3+}, Zn^{2+}	$9.7x10^{-6}$ $3.65x10^{-6}$	14

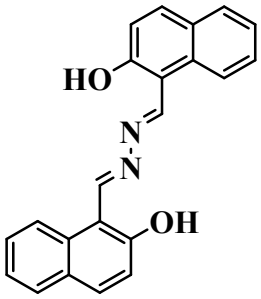	Yes	No	Cu^{2+}	$1.1x10^{-7}$	15
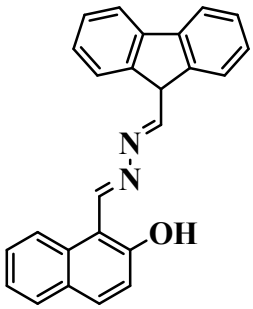	Yes	No	No	-------	16
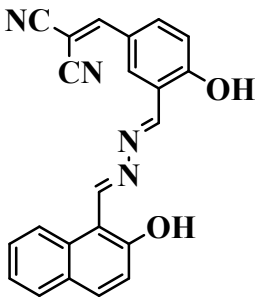	Yes	No	Cu^{2+}	2.5×10^{-9}	17
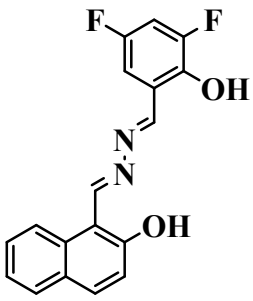	**Yes**	**Both Mechanochromic and Acidochromic**	**Cu^{2+}**	**$0.71x10^{-6}$**	**This Work**

1. M.K. Nayak, Synthesis, characterization and optical properties of aryl and diaryl substituted phenanthroimidazoles, J. Photochem. Photobiol. A Chem. 241 (2012) 26–37.

2. A.I. Ciuciu, K. Skonieczny, D. Koszelewski, D.T. Gryko, L. Flamigni, Dynamics of intramolecular excited state proton transfer in emission tunable, highly luminescent imidazole derivatives, J. Phys. Chem. C 117 (2013) 791–803.

3. A.D. Becke, Density-functional thermochemistry. III. The role of exact exchange, J. Chem. Phys. 98 (1993) 5648–5652.

4. P.J. Stephens, F.J. Devlin, C.F. Chabalowski, M.J. Frisch, Ab initio calculation of vibrational absorption and circular dichroism spectra using density functional force fields, J. Phys. Chem. 98 (1994) 11623–11627.

5. X.-J. Yan, Z.-G. Wang, Y. Wang, Y.-Y. Huang, H.-B. Liu, C.-Z. Xie, Q.-Z. Li, J.-Y. Xu, A dual-functional fluorescent probe for sequential determination of Cu2+/S2 and its applications in biological systems, Spectrochim. Acta Part A Mol. Biomol. Spectrosc. 243 (2020) 118797.

6. H.A. Benesi, J.H. Hildebrand, A spectrophotometric investigation of the interaction of iodine with aromatic hydrocarbons, J. Am. Chem. Soc. 71 (1949) 2703–2707.

7. J.R. Lakowicz, Principles of Fluorescence Spectroscopy, Springer, 2006.

8. Yadav, Richa, et al. "A viscochromic, mechanochromic, and unsymmetrical azine for selective detection of Al 3+ and Cu 2+ ions and its mitotracking studies." *New Journal of Chemistry* 43.18 (2019): 7109-7119.

9. Bhardwaj, Vinita, SK Ashok Kumar, and Suban K. Sahoo. "Fluorescent sensing (Cu2+ and pH) and visualization of latent fingerprints using an AIE-active naphthaldehyde-pyridoxal conjugated Schiff base." *Microchemical Journal* 178 (2022): 107404.

10. Shen, Lingyi, et al. "Naphthaldehyde-based Schiff base dyes: aggregation-induced emission and high-contrast reversible mechanochromic luminescence." *Materials Chemistry Frontiers* 6.17 (2022): 2491-2498.

11. Arshad, Muhammed, et al. "Highly sensitive detection of copper in aqueous media using a fluorescent probe developed from isophthaldehyde and (E)-1-(hydrazonomethyl) naphthlen-2-ol." *Sensors and Actuators A: Physical* 373 (2024): 115436.

12. Arshad, Muhammed, Anila Paul, and Abraham Joseph. "Nanoscale detection of copper using an aggregation induced emission enhancement fluorescent sensor derived from hydroxy naphthaldehyde and benzyloxy benzaldehyde." *Journal of Photochemistry and Photobiology A: Chemistry* 444 (2023): 114983.

13. Goswami, Nilotpal, Himadri Priya Gogoi, and Pranjit Barman. "A hydrazine-based unsymmetrical bis-imine-Schiff base as a chemosensor for turn-off fluorescence and naked-eye detection of Cu2+ ion: application in aqueous media using test strips." *Journal of Photochemistry and Photobiology A: Chemistry* 446 (2024): 115106.

14. Das, Bhriguram, et al. "Solvent-regulated fluorimetric differentiation of Al3+ and Zn2+ using an AIE-active single sensor." *The Journal of Physical Chemistry A* 125.7 (2021): 1490-1504.

15. Liu, B., Zhou, H., Yang, B., & Hu, X. (2017). Aggregation–induced emission activity and further Cu2+-induced self-assembly process of two Schiff compounds. *Sensors and Actuators B: Chemical*, *246*, 554-562.

16. Taneja, S., Sharma, K., Selvam, P., Kumar, S. A., Thiruppathi, G., Sundararaj, P., & Ramasamy, S. K. (2024). Highly Potent Fluorenone Azine-based ESIPT Active

Fluorophores for Cellular Viscosity Detection and Bioimaging Applications. *Journal of Fluorescence*, 1-15.

17. Haloi, Pankaj, et al. "Effect of structural variation on AIE behavior: A case study of salicylaldehyde-naphthaldehyde-azine based of meta fluorophore." *Spectrochimica Acta Part A: Molecular and Biomolecular Spectroscopy* (2025): 127204.